Online Material

1.0 Analytical methods

High spatial resolution textural observations and some semi-quantitative mineral chemical data on SMB biotites were obtained using a TESCAN MIRA 3 LMU Variable Pressure Schottky Field Emission Scanning Electron Microscope (SEM) at Saint Mary's University. The SEM is equipped with a 80 mm^2 X-max Oxford Instruments EDS detector and a back-scattered electron (BSE) detector. X-ray mapping and emi-quantitative analyses were done using INCA software. A beam voltage of 20 kV, beam current of 0.2 nA and an approximate working distance of 17 mm were used for all EDS spot analyses, X-ray mapping and imaging.

The major element composition of biotite was determined using the JEOL JXA-8200 Electron Probe Micro-Analyzer (EPMA) housed in the Robert M. MacKay Electron Microprobe Lab at Dalhousie University. Biotite analyses were done using an accelerating voltage of 15kV, a beam current of 20 nA, and a 1 µm focused beam to limit sample damage. Standards for biotite analysis were biotite (Fe, Al, Si, K, Mg), pyrolusite (Mn), kaersutite (Ca, Ti), albite (Na), tugtupite (Cl) and apatite (F). Count times were 50 seconds on peak for F and 20 seconds on peak for all other elements. The spectral interference from the Fe $L\alpha_{1,2}$ emission line (705 eV) on the F kα line (676.8 eV) was determined by measuring the F kα intensity in Fe-metal, which was then used to calculate an appropriate correction factor. Analysis of natural hematite yielded F concentrations of $\leq$ 0.02 wt%, confirming the efficacy of this correction method. A full list of sample analyses is provided in Table S1.

Samples that had not been previously collected and analysed as part of historical Nova Scotia Department of Natural Resources and Renewables bedrock mapping and geochemistry initiatives (all samples with 18JC and 19BM prefixes) were analysed by ICP-MS at Actlabs (Ancaster, Ontario, Canada) using the 4LITHO analysis package. This involved initial crushing, then pulverizing with mild steel to 95%

passing 74 micrometers. Pulverized samples were then fused with lithium metaborate/tetraborate, then rapidly digested in weak nitric acid. This method was used to ensure complete dissolution of refractory mineral phases. A summary of major and trace element whole-rock analyses of these samples, as well as analyses from the Department of Natural Resources and Renewables database and external standard reference materials, is provided in Tables S2 and S3.

2.0 MELTS modeling of the biotite Fe# vs wt% Ti systematics

Consistent with Bucholz et al (2018), we used the alphaMELTS version 1.6 (Smith and Asimow, 2005), which employs the biotite thermodynamic data and solution model from McMullin et al. (1991). We selected two compositions to model, samples 18JC-0008 (Halifax Pluton; whole-rock Fe# =0.65) and A16-3052 (Fishtail Pluton; whole-rock Fe# = 0.52), both contain biotite with high Ti and low Fe#, and span the range in whole-rock Fe# for the least evolved (i.e., lowest SiO_2, highest TiO_2) samples measured in this study. A crystallization pressure of 300 MPa was assumed, which is within the range of 240 to <470 MPa for the current level of SMB exposure based on the evidence discussed in section 4.3.1. of the main text. Models were run in fractional crystallization mode at water saturated conditions, with an initial temperature of 1100 ^{o}C. Biotite is saturated at 984-986 ^{o}C and 944-954 ^{o}C in the FIP and HP compositions, respectively, and continues to crystallize to 664^{o}C, at which point the models were terminated with 10% liquid remaining. The range in biotite-in temperatures reflects a decrease with increasing fO_2. The MELTS model does not calculate the Ti content of biotite, which instead was determined using the melt Ti content combined with the biotite/melt partition coefficient of 24, measured in experiments on peraluminous compositions by Icenhower and London (1995).

3.0 Estimation of biotite-melt K_D for OH-F and OH-Cl exchange

Here we follow the formalism of Li and Hermann (2015) for calculating the relevant biotite-melt exchange coefficients, using the experimental results of Icenhower and London (1997). We briefly outline the Li and Herman (2015) method here, but refer the reader to their Appendix C for full details of calculating the melt species mole fractions. The biotite-melt exchange of OH, F and Cl components can be expressed by the heterogeneous reactions:

$$\text{Biotite(F)} + M_{1/x}OH_{(melt)} = \text{Biotite(OH)} + M_{1/x}F_{(melt)} \qquad \text{(S1)}$$

$$\text{Biotite(Cl)} + M_{1/x}OH_{(melt)} = \text{Biotite(OH)} + M_{1/x}Cl_{(melt)} \qquad \text{(S2)}$$

in which $M_{1/x}F_{(melt)}$, $M_{1/x}OH_{(melt)}$ and $M_{1/x}Cl_{(melt)}$ refer to metal-anion species in the melt, of metal valence x. The resulting exchange coefficients, K_D, are:

$$K_D(\text{OH-F}) = X_{OH}^{biot} * X_F^{melt} / X_F^{biot} * X_{OH}^{melt} \qquad \text{(S3)}$$

$$K_D(\text{OH-Cl}) = X_{OH}^{biot} * X_{Cl}^{melt} / X_{Cl}^{biot} * X_{OH}^{melt} \qquad \text{(S4)}$$

The OH, F and Cl components in the biotite (X_{OH}^{biot}, X_F^{biot}, X_{Cl}^{biot}) are calculated on the basis of 22 O, F and Cl, with OH determined by stoichiometry. Li and Hermann (2015) modeled the melt components (X_{OH}^{melt}, X_F^{melt}, X_{Cl}^{melt}) assuming that hydrous silicate melts are ideal mixtures of H_2O molecules (H_2O_{melt}), OH groups (OH_{melt}) and oxygen atoms (O_{melt}), consistent with the results of Silver and Stolper (1985). The proportion of these species can be calculated by combining mass balance with the equilibrium constant (K_{H2O}) for the homogeneous exchange reaction:

$$H_2O_{melt} + O_{melt} = 2OH_{melt} \qquad \text{(S5)}$$

In which the activities of the melt species are expressed as mole fractions, yielding the relation:

$$K_{H2O} = (X_{OH}^{melt})^2 / (X_{H2O}^{melt} * X_{O}^{melt}) \qquad (S6)$$

The value of the equilibrium constant, K_{H2O}, is calculated from the experiments of Zhang et al. (1997), using their relation:

$$\ln K_{H2O} = 1.88 - 3100/T \qquad (S7)$$

in which T is in Kelvin. Li and Hermann (2015) also assumed that F and Cl substitute for bridging oxygens in the silicate melt network, and that mixing is ideal, such that the activities of the Cl and F species are equal to their mole fractions.

Experimental data on biotite-melt partitioning of the halogens is limited to only a few studies in which full compositional data on biotite and melt are provided. These include the experiments of Icenhower and London (1997), Lukkari and Holtz (2007), Chevychelov et al. (2008) and Zhang et al (2022). Icenhower and London (1997) conducted experiments at 200 MPa, 640-680°C, FMQ + 0.5, using the peraluminous Spor Mountain vitrophyre (Utah, USA), producing melts with molar $Al_2O_3/(CaO + Na_2O + K_2O)$, or A/CNK, of 1.1-1.2. The principal experimental variable investigated was the change in F and Cl partitioning with biotite Fe#, reflecting the importance of Mg-Cl and Fe-F avoidance on the uptake of these elements. Lukkari and Holtz (2007) measured phase equilibrium involving the peraluminous Kymi topaz granite (Finland) at 200 MPa, 625-700°C and ~FMQ+0.5 doped with up to 5 wt% F, which produced melts with A/CNK of 1.2-1.4. Owing to the lack of MgO in the starting composition, the resulting biotite corresponds to the pure Fe endmember. The experiments of Chevychelov et al. (2008) employed the synthetic equivalent of Mt Vesuvius (Italy) phonolite and experimental conditions of 200 MPa, 850°C and fO_2 of ~FMQ+0.5, with run-product melts having A/CNK = 0.8-0.9. Experiments were designed to measure biotite-melt partitioning between melt and aqueous fluid as a function of F and Cl concentration, in which biotite compositions were held constant at an Fe# of ~0.5. Other experiments reported by LaTourrette et al. (1995) and Righter and Carmichael (1996) measured trace element

partitioning and phase equilibrium involving Mg-rich biotite compositions (<10% FeO in run-product biotites) and mafic alkalic melt compositions (A/CNK = 0.5-0.6) at 900-1300^{o}C, and 0.1 MPa to 2 GPa over a significant range of fO_2 (FMQ to FMQ + 6). Zhang et al. (2022) combined data from these aforementioned studies along with their own additional measurements at 100-500 MPa, 850-975^{o}C involving a range of melt compositions to develop a regression for K_D as a function of biotite and melt compositional parameters. However, their regression fails to fully describe any dependence of K_D for OH-Cl exchange on the Fe# of biotite, as documented by Icenhower and London (1997); this is considered essential for an accurate description of chlorine behavior in the context of degassing. Since the P-T-fO_2 and melt composition employed in the Icenhower and London (1997) study is a reasonable proxy for the SMB, and owing to the relatively strong role of biotite composition on partitioning, we chose to use that data for parameterizing the K_Ds employed in modeling. K_D-values from the Icenhower and London (1997) experiments were calculated after the method described above, and are portrayed as a function of the molar Fe/(Mg+Fe) of biotite (X_{Fe}^{biot}) in Figure S1. The K_D show sympathetic changes with biotite composition, with K_D OH-F increasing, and OH-Cl decreasing as X_{Fe}^{biot} increases. Weighted least squares linear fits to the data define the following equations:

$$\text{Log } K_D \text{ OH-F} = -1.8005(\pm 0.0116) + 1.9314(\pm 0.0270)\times 10^{-2}(100 * X_{Fe}^{biot}) \quad r = 0.9804 \quad \text{(S8)}$$

$$\text{Log } K_D \text{ OH-Cl} = -0.38592(\pm 0.12506) - 6.406(\pm 2.324) \times 10^{-3}(100 * X_{Fe}^{biot}) \quad r = 0.61506 \quad \text{(S9)}$$

The scatter, and poorer fit, to the K_D OH-Cl data reflects the much lower concentration of chlorine in the natural composition that was employed by Icenhower and London (1997). The temperature dependence of log K_D is assumed to be the same as for biotite-fluid exchange as summarized in Munoz (1984). Although Lukkari and Holtz (2007) measured K_D(OH-F) for Fe endmember biotite over the temperature range of 625-700^{o}C, this temperature interval is too small and their data are too imprecise to extract a meaningful slope. In support of our approach, Riker et al. (2018) regressed all of the

available apatite-melt values of K_D(OH-F, Cl) as a function of temperature, and determined slopes that are essentially identical to those determined for apatite-fluid exchange. Incorporating the biotite-fluid temperature dependence into equations S8 and S9 yields:

$$\text{Log } K_D \text{ OH-F} = 2100/TK - 4.051304(\pm 0.0116) + 1.9314(\pm 0.0270) \times 10^{-2}(100 * X_{Fe}^{biot}) \quad \text{(S10)}$$

$$\text{Log } K_D \text{ OH-Cl} = 5151/TK - 5.90682(\pm 0.12506) - 6.406(\pm 2.324) \times 10^{-3}(100 * X_{Fe}^{biot}) \quad \text{(S11)}$$

which are the equations used in modeling the SMB dataset.

In terms of validating the model, we first compare the calculated vs measured X_F^{biot}, X_{Cl}^{biot} and X_{OH}^{biot} for the calibrating dataset in Figure S2, which shows that the measured biotite compositions from Icenhower and London (1997) are reproducible, mostly within analytical error, using equations S10 and S11. In terms of other results, Lukkari and Holtz (2007) conducted experiments involving a peraluminous melt composition at the P-T conditions similar to Icenhower and London (1997). Calculated vs measured biotite compositions from the experiments of Lukkari and Holtz (2007) are shown in Figure S3. In this case, all the biotites are Mg-free, so the only parameter varied in those experiments is the fluorine content of the experiment and temperature. As shown in Figure S1, the calculated K_D(OH-F) from those experiments is lower than the value extrapolated from the Icenhower and London (1997) X_{Fe} vs K_D relations, resulting in calculated X_{OH}^{biot} and X_F^{biot} that are somewhat higher and lower, respectively, than measured (Figure S3), although the relative proportions of the two components are correct. It is not clear as to the origin of the discrepancy between the calculated and measured compositions, although it is worth noting that Lukkari and Holtz (2007) do not report any correction to their fluorine analyses from the spectral interference of the Fe $L\alpha_{1,2}$ emission on the F $K\alpha$ line. Given the iron-rich nature of the biotite produced in their experiments, this lack of correction would result in an overestimation of the fluorine concentration, and a shift to higher X_F and lower X_{OH} than model predictions.

4.0 Constraints on fluid/melt partitioning of chlorine

A significant variable that affects chlorine partitioning is the total chlorine content of the melt phase, with values of $D_{Cl}^{vap/melt}$ increasing with increasing Cl concentration (Baker and Alletti, 2012). However, at Cl concentrations below ~500 μg/g, partitioning is constant, and results within that concentration range are considered relevant to modeling the SMB. Partition coefficients involving haplogranite (A/CNK ~1) and phonolite compositions define a systematic increase in $D_{Cl}^{vap/melt}$ with increasing pressure (Shinohara et al., 1989; Signorelli and Carroll, 2000), which is the basis for the calibration presented in Cline and Bodnar (1991) used in modeling the origins of porphyry copper deposits, and applied by other workers subsequently. Values of $D_{Cl}^{vap/melt}$ used in that calibration are generally higher than reported by other workers (Baker and Alletti, 2012) and indeed would produce unrealistically large Cl depletions by MVP removal in the modeling presented in this study. We have instead parameterized the experimental data of Webster and Holloway (1988) from experiments done using a peraluminous rhyolite composition at 200 and 500 MPa, 800-950°C and total Cl in the melt of $\leq$400 μg/g. The data are portrayed in Figure S4, with the resulting best fit defining the relation:

$$D_{Cl}^{vap/melt} = 6.9889 + 0.0327*P(MPa) \qquad r = 0.753 \qquad (S12)$$

at 300 MPa yielding a value of $D_{Cl}^{vap/melt}$ = 17, which is used in the models.

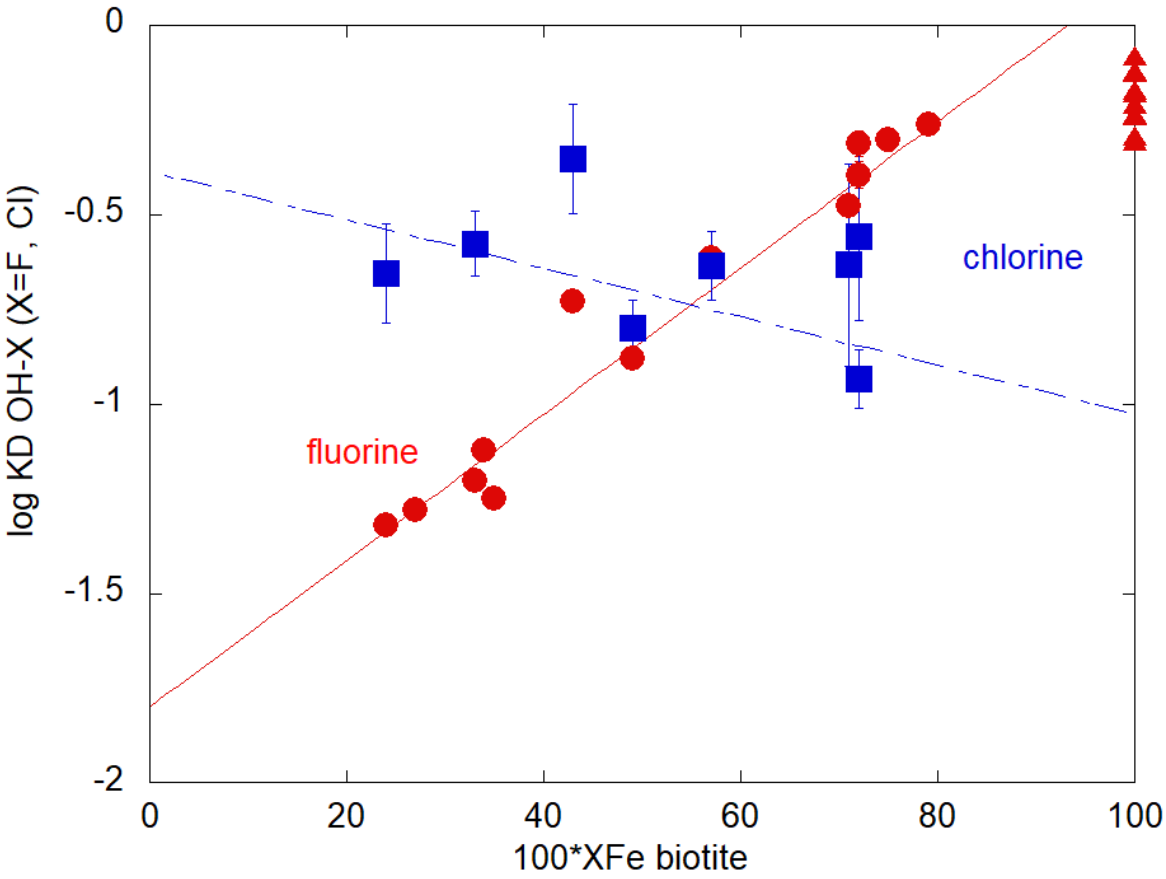

Figure S1. Log of the calculated biotite-melt exchange coefficients (K_D) for F-OH and Cl-OH as a function of the molar Fe/Mg+Fe of biotite from experiments done by Icenhower and London (1997) at 200 MPa, 640-680°C and fO_2 of ~FMQ+0.5 (filled circles and squares) and Lukkari and Holtz (2007) at the same pressure and fO_2, and 625-700°C (filled triangles), both involving peraluminous melt compositions. Regression curves are weighted least squares fits to the Icenhower and London (1997) data, corresponding to equations S8 and S9 in the text.

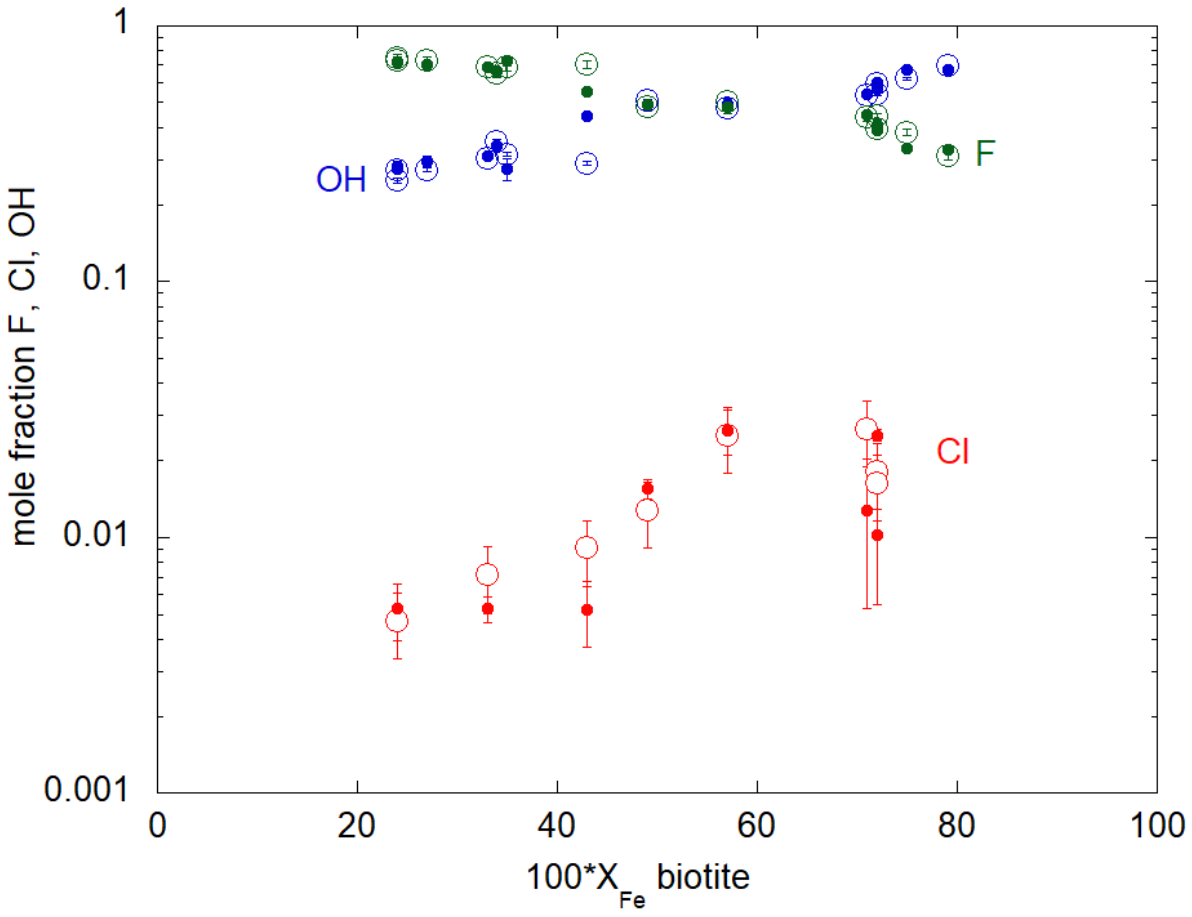

Figure S2. Comparison between the model (open symbols) and measured (solid symbols) biotite compositions produced in the experiments of Icenhower and London (1997) involving a peraluminous melt composition (A/CNK = 1.1-1.2) at 200 MPa, 625-700°C and fO_2 of ~FMQ+0.5. Model biotite compositions were calculated from the measured Cl, F and H_2O concentrations in the melt phase, biotite X_{Fe}, experiment temperature and equations S10 and S11 in the text. Error bars for the calculated values are propagated through equations S10 and S11. Error bars on the measured values are based on the standard deviation of multiple measurements.

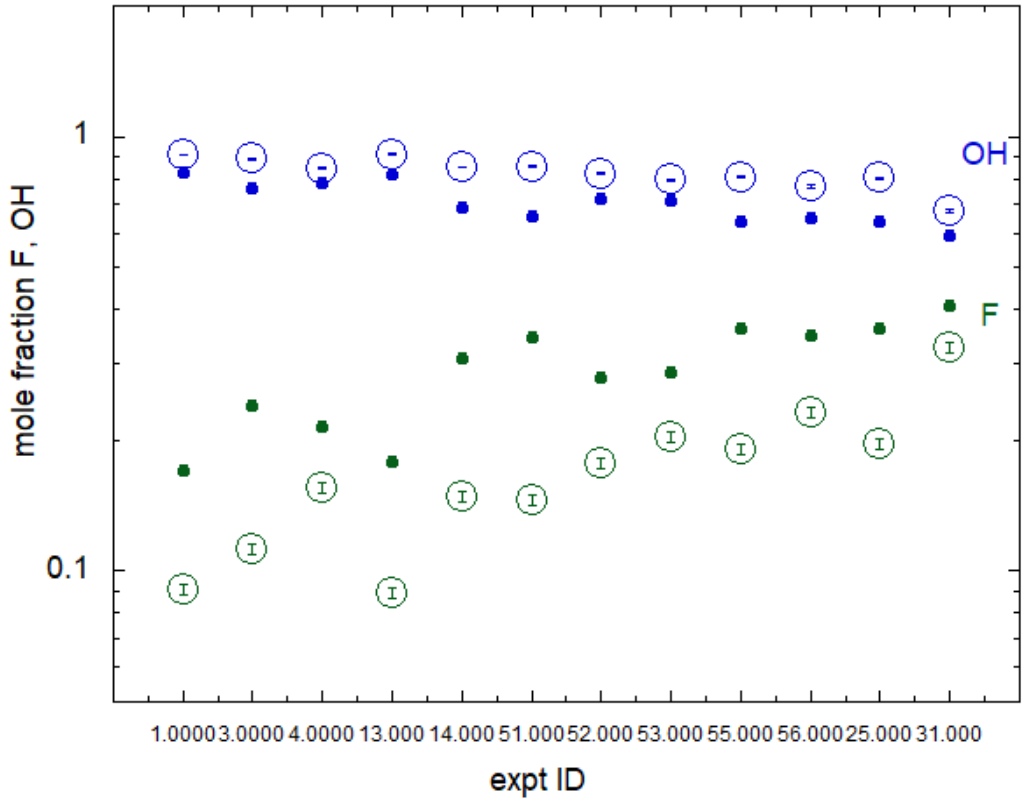

Figure S3. Comparison between the model (open symbols) and measured (solid symbols) biotite compositions from the experiments of Lukkari and Holz (2007) involving a Cl- and MgO-free, peraluminous melt composition (A/CNK = 1.1-1.2) at 200 MPa, 625-700°C and fO_2 of ~FMQ+0.5. Model biotite compositions were calculated from the measured F and H_2O concentrations in the melt phase, biotite X_{Fe}, experiment temperature and equations S10 and S11 in the text. Error bars for the calculated values are propagated through equations S10 and S11. In the original reference, errors were not reported for biotite compositions.

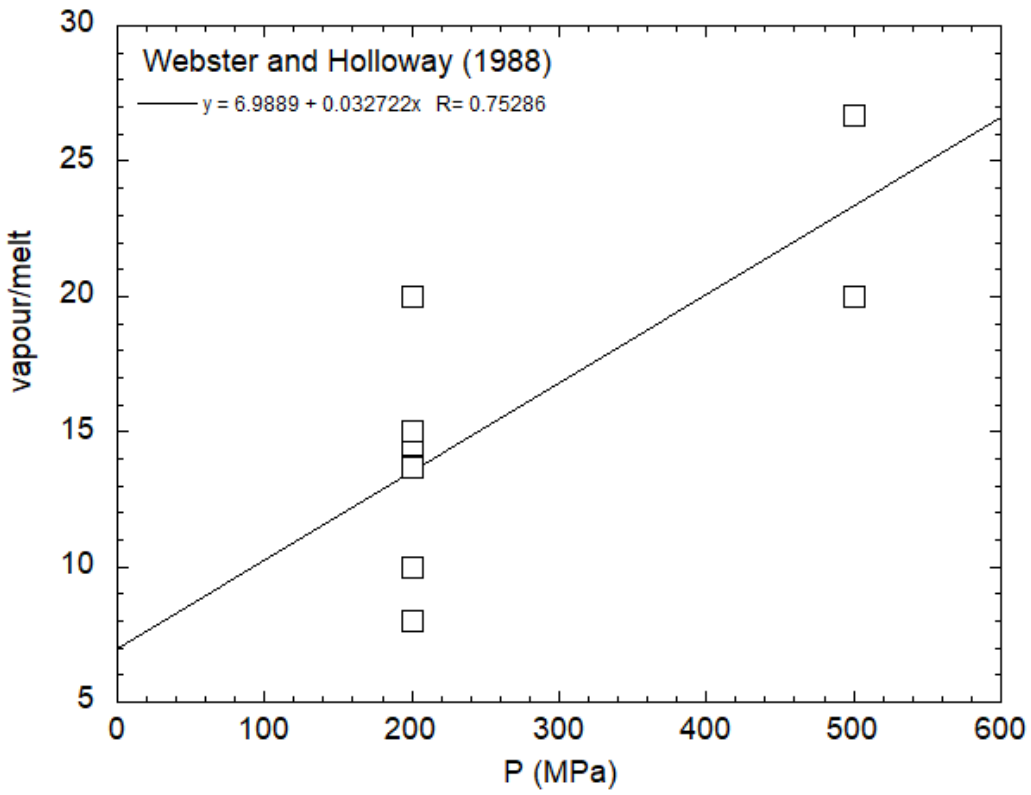

Figure S4. Fluid/melt partition coefficients for chlorine as a function of pressure reported by Webster and Holloway (1988) for experiments done at 800-950^{o}C involving silicate melts with A/CNK of 1.05 to 1.23 and $\leq$ 400 ug/g chlorine.

Online Material References

Baker, D.R. and Alletti, M. (2012) Fluid saturation and volatile partitioning between melts and hydrous fluids in crustal magmatic systems: The contribution of experimental measurements and solubility models. *Earth-Science Reviews*, vol 114, pp 298-324.

Bucholz, C.E., Stolper, E.M., Eiler, J.M. and Breaks, E.W. (2018) A Comparison of Oxygen Fugacities of Strongly Peraluminous Granites across the Archean– Proterozoic Boundary. *Journal of Petrology*, vol 59, pp 2123-2156.

Cline J.S.and Bodnar R.J. (1991) Can economic porphyry copper mineralization be generated by a typical calc-alkaline melt? *Journal of Geophysical Research* vol 96, pp 8113-8126.

Chevychelov, V.Y., Botcharnikov, R.E. and F. Holtz F. 2008) Experimental study of fluorine and chlorine contents in mica (biotite) and their partitioning between mica, phonolite melt, and fluid. *Geochemistry International*, Vol. 46, pp. 1081–1089.

Icenhower, J. and London, D. (1997) Partitioning of fluorine and chlorine between biotite and granitic melt: experimental calibration at 200 MPa H2O. *Contributions to Mineralogy and Petrology*, vol 127, pp 17–29.

LaTourrette T, Hervig RL and Holloway JR (1995) Trace element partitioning between amphibole, phlogopite, and basanite melt. *Earth and Planetary Science Letters*, vol 135, pp 13–30.

Li L. and Hermann, J. (2015) Apatite as an indicator of fluid salinity: An experimental study of chlorine and fluorine partitioning in subducted sediments. *Geochimica et Cosmochimica Acta*, vol 166, pp 267–297.

Lukkari S. and Holtz F. (2007) Phase relations of a F-enriched peraluminous granite: An experimental study of the Kymi topaz granite stock, Southern Finland. *Contrib. Mineral. Petrol,* vol 153, pp 273–288.

McMullin, D. W., Berman, R. G. & Greenwood, H. J. (1991). Calibration of the SGAM thermobarometer for pelitic rocks using data from phase-equilibrium experiments and natural assemblages. *Canadian Mineralogist* vol 29, pp 889–908.

Munoz, J.L. (1984) F–OH and Cl–OH exchange in micas with applications to hydrothermal ore deposits. In Micas, *Reviews in Mineralogy*, Mineralogical Society of America, pp. 469–493.

Riker, J., Humphreys, M.C.S., Brooker, R.A., De Hoog, J.C.M. and EIMF (2018) First measurements of OH-C exchange and temperature-dependent partitioning of OH and halogens in the system apatite–silicate melt. *American Mineralogist*, vol 103, pp 260-270.

Righter, K. and Carmichael, I.S.E. (1996) Phase equilibria of phlogopite lamprophyres from western Mexico: biotite-liquid equilibria and P-T estimates for biotite-bearing igneous rocks. *Contributions to Mineralogy and Petrology*, vol 123, pp 1-21.

Shinohara, H., Iiyama, J.T., and Matsuo, S. (1989) Partition of chlorine compounds between silicate melt and hydrothermal solutions. *Geochimica et Cosmochimica Acta* vol 53, pp 2617–2630.

Silver L. and Stolper E. (1985) A thermodynamic model for hydrous silicate melts. *Journal of Petrology* vol 93, pp 161-177.

Signorelli, S., Carroll, M.R., 2000. Solubility and fluid–melt partitioning of Cl in hydrous phonolitic melts. *Geochimica et Cosmochimica Acta* 64, 2851–2862.

Smith, P. M. & Asimow, P. D. (2005). Adiabat_1ph: a new public front-end to the MELTS, pMELTS, and pHMELTS models. Geochemistry, Geophysics, Geosystems 6, Q02004.

Webster, J.D. and Holloway, J.R., 1988. Experimental constraints on the partitioning of Cl between topaz rhyolite melt and H_2O and H_2O+CO_2 fluids: new implications for granitic differentiation and ore deposition. *Geochimica et Cosmochimica Acta* vol 52, pp 2091–2105.

Webster, J.D., Goldoff, B.A., Flesch, R.N., Nadeau, P.A. and Silbert, Z.W. (2017) Hydroxyl, Cl, and F partitioning between high-silica rhyolitic melts-apatite-fluid(s) at 50-200 MPa and 700-1000 degrees C. *American Mineralogist*, vol 102, pp 61-74.

Zhang Y., Belcher R., Ihinger P. D., Wang L., Xu Z. and Newman S. (1997) New calibration of infrared measurement of dissolved water in rhyolitic glasses. *Geochimica et Cosmochimica Acta* vol 61, pp. 3089–3100.